Qin *et al.*
Chinese Journal of Mechanical Engineering (2023) 36:107
https://doi.org/10.1186/s10033-023-00938-x

Chinese Journal of Mechanical Engineering

ORIGINAL ARTICLE

Open Access

Surface Characterization and Tribology Behavior of PMMA Processed by Excimer Laser

Dong Qin[1,2], Juan Guo[2], Ming Liang[2], Ling Chen[2] and Weimin He[1*]

Abstract

Polyoxymethylene methacrylate (PMMA) is widely used in ophthalmic biomaterials. Misuse of PMMA in extreme environments is likely to damage the ocular surface and intraocular structures. The surface characterization and tribological behavior of PMMA processed using an excimer laser were investigated in this study by contrasting different lubrication conditions and friction cycles. The results show that the roughness of the material surface increases with laser processing, which changes its physical structure. Under lubrication, the laser-treated PMMA exhibits better hydrophilicity, especially during the use of eye drops. No obvious relationship exists between the laser-processing time and friction behavior. However, the laser treatment may contribute to the formation of friction and wear mechanisms of PMMA materials. Laser-treated PMMA in saline solution exhibits better abrasive resistance by showing a lower wear rate than that in eye drops, although it has a higher friction coefficient. In this study, the different friction stages in laser-treated PMMA were clarified under two lubrication conditions. The wear rates of the laser-treated PMMA were found to decrease with the number of cycles, and the friction coefficient has a similar variation tendency. The wear behavior of the laser-treated PMMA is dominated by the main abrasive wear and secondary transferred film formation. This study provides a theoretical basis for the development and application of ophthalmic biomaterials in complex environments by examining the material surface interface behavior and wear mechanism after laser processing using PMMA as the research matrix.

Keywords Biocompatible materials, Poly (methyl methacrylate), Surface characterization, Tribology behavior

1 Introduction

The use of polymer materials has become a major challenge in sustainable global human development and environmental protection [1]. Their mechanical, thermal, and photoacoustic magnetic separation, degradation, and processing properties enable polymer materials to contribute to the aviation, aerospace, nuclear, medicine, and health industries. The design, production, and application of polymer materials have received considerable attention [2]. Their flexible design characteristics strongly support the development of society in diverse ways. Thus, the composition, processing, structure, and nature of polymer materials are constantly being improved. Medical polymers are an important class of polymer materials used in medical applications, such as *in vitro* diagnosis, drug-sustained release, regenerative medicine, implant and interventional devices, and tissue engineering [3–5]. By 2023, the global market potential for biological implants is expected to reach approximately US$ 12415.4 billion (compound annual growth rate of 6.3%) [6].

For a long time, the treatments of eye diseases, healthcare, and beauty have been an important part of the medical field in which ophthalmic medical polymer materials are widely used. Polyoxymethylene methacrylate (PMMA) was the earliest and is the most widely used polymer material because of its high light transmittance (92%) resulting from such advantages as better

*Correspondence:
Weimin He
hewm888@hotmail.com
[1] Department of Ophthalmology, West China Hospital, Sichuan University, Chengdu 610000, China
[2] Ophthalmology Department, The Third People's Hospital of Chengdu, Chengdu 610031, China

refractive index, stable properties, and convenient processing [7]. PMMA was first discovered by British chemists Roland Hill and John Crawford in the early 1930s and was first applied by German chemist Otto Romm in 1934 [8]. PMMA is widely used in various fields of production and daily life, such as national defense, aerospace, the machinery and chemical industries, automotive instrumentation, building decoration, and medical equipment [9]. It is also used in biomedical applications such as polymer electrolytes, polymer viscosity, electrodiffusion, and electroosmotic flow [10–14]. It is an excellent light transmitting material for treating eye damage that requires the implantation of artificial substitutes, such as artificial corneas, artificial lenses, artificial tears, hidden glasses, glasses, and goggles [15].

PMMA was first used to create intraocular lenses (IOLs). Long-term clinical observation revealed that PMMA is an ideal IOL material with stability, light weight, satisfactory transparency, a refractive index of 1.49, high resistance to aging and environmental changes, strong acid, alkali, and organic solvent resistance, and high biocompatibility. However, owing to material limitations, PMMA has disadvantages, such as high hardness, difficulty in measuring intraocular pressure after implantation, uncomfortable initial wear, poor adhesion of epidermal cells, risk of latent infection, leakage, and keratolysis after surgery, and low oxygen permeability [16]. Hence, researchers [17] have applied numerous methods to modify the material surface.

To improve the moisturizing properties of PMMA, researchers [16, 18–20] have modified the surface of the material to improve its moisturizing performance and increase its oxygen permeability. With the development of science and technology, ophthalmic materials have become more widely used and have become increasingly in demand for objects used in extreme environments, causing lesions, damage, and even permanent disability in the eyes. Thus, researchers have conducted extensive studies on the radiation effects of various materials under different types of ion irradiation [21–24]. In addition to the diseased site, normal tissues and organs are irradiated with ionizing radiation, which causes various degrees of side effects [25]. Previous studies have shown that ultraviolet (UV) light has a photochemical effect on tissues, inducing excessive production of free radicals and lipid peroxides in cell membranes and thereby impairing the functioning of multiple organs in the eye [26].

However, under normal circumstances, humans are rarely exposed to extreme environmental conditions without eye protection. Thus, strengthening the development of eye protection facilities in extreme environments is particularly important. These materials must first be able to exist in extreme environments. Artificially accelerated PMMA damage is used to simulate the laser radiation of materials based on the damaged material surface interface behavior, friction, and wear regulation mechanism. The excimer laser output is primarily concentrated in the UV band, and the low density of the working medium reveals its unique advantages for magnifying ultrashort pulses. Common excimer lasers used for UV ultrashort-pulse amplification are XeCl, KrF, and ArF, with central wavelengths of 308, 248, and 193 nm, respectively [27]. The ArF excimer laser is a commonly used form of laser therapy in ophthalmology. It is a cold laser, and its short pulse duration, small thermal effect, surface concentration, high efficiency, and low-damage processing provide advantages in the field of fine precision processing [28–30].

To study systematically the surface behavior and friction wear performance change of PMMA after laser damage in a liquid environment, normal saline solution and eye drops at room temperature and the eye surface environment were chosen, and PMMA ArF laser irradiation was used. The surface morphology changes were then examined, and a SiC ball was used as the friction pair to study the wear performance of the materials in a friction wear environment. A comparative analysis was used to evaluate the changes in the PMMA, interface behavior, and wear performance after injury. Most products are currently manufactured by enterprises outside China. China is still in the research and development stage for synthetic polymers and remains unable to produce medical products independently. Thus, the localization of high-quality products is an urgent problem that must be solved.

2 Materials and Methods

2.1 Materials and Sample Preparation

Commercial PMMA (model brand: Shengmei) was selected as the target material. All the specimens were prepared with a length, width, and thickness of 35, 20, and 5 mm, respectively. The PMMA surface was cleaned with deionized water before irradiation to remove impurities and ensure the reliability of the experimental measurement data.

The laser processing is shown in Figure 1. The WaveLight EX500 is a stationary scanning spot stimulated excimer laser system used in refractive surgery. The maximum laser terminal output energy of the laser device is <5 mJ, the pulse width is 6 ± 1 ns, the therapeutic laser wavelength is 193 ± 5 nm, and the beam energy of the laser has a Gaussian distribution. The design scanning diameter was 6.0 mm, the scans were performed at seven treatment times (t = 2, 7, 13, 18, 23, 28, and 33 s), and the spot size of the surgical area was 0.95 ± 0.15 mm.

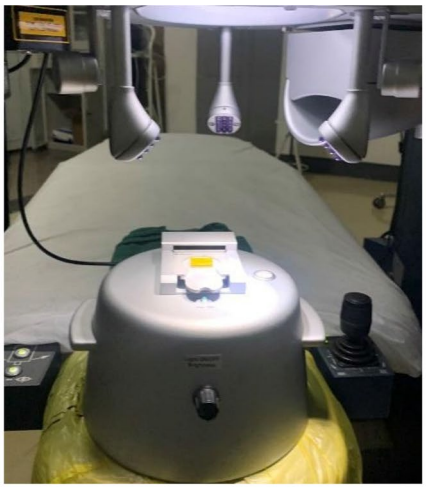

(a) Laser device

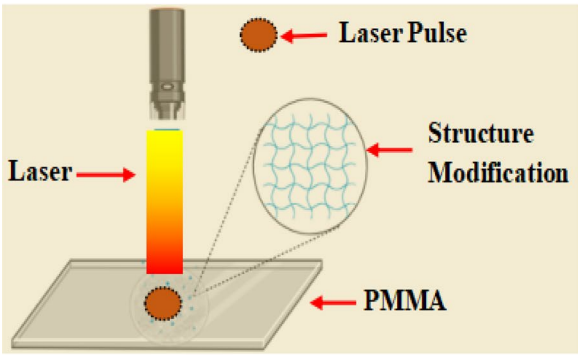

(b) Schematic

Figure 1 Photograph of device and schematic of laser treatment processing

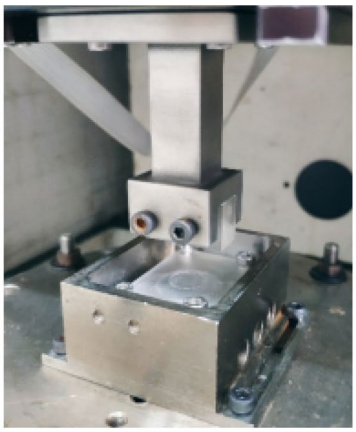

(a) Fixture

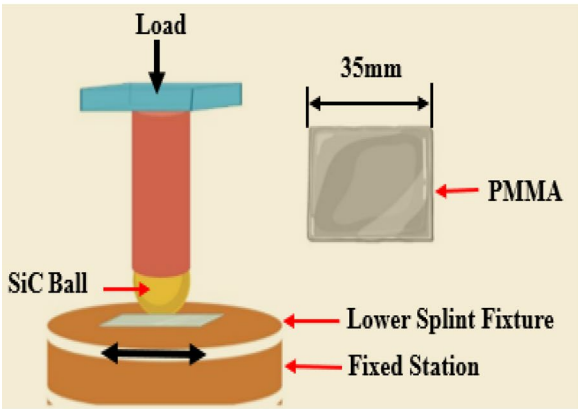

(b) Diagrammatic sketch

Figure 2 Specimen and the friction and wear test

2.2 Experimental Equipment Parameters

2.2.1 Characterization Analysis

The morphology was observed using a white-light interferometer (SuperView W1) to characterize the three-dimensional (3D) topography and obtain a drawing of the wear scars. To determine the surface wettability of the PMMA samples, solid–liquid contact angles were measured using an optical contact angle measuring instrument (SDC-350). The microstructure was characterized using a scanning electron microscope (Tungsten Filament Scanning JEM [JSM-IT500]). The materials were analyzed based on their Raman spectra (Lab Ram HR).

2.2.2 Friction and Wear Tests

Friction and wear tests of the laser-treated PMMA were performed using a homemade fretting wear rig, as shown in Figure 2. The fixture supporting the PMMA had two parts: an upper splint and a lower splint, as shown in Figure 2. The upper splint was a ϕ8 mm SiC ball. A flat sample was locked under a lower splint fixture and discharged onto smooth rail assemblies. The upper splint, lower splint, and test box were connected by screws, and the PMMA was fixed in the fixture containing the experimental medium. The SiC ball was held by an upper sample holder and slowly approached the PMMA surface. A load of 10 N and a number of moving cycles were applied to achieve the desired experimental conditions. The experimental parameters are listed in Table 1. After

Table 1 The experimental parameters of the wear test

Test parameters	
Laser processing time	2 s, 7 s, 13 s, 18 s, 23 s, 28 s, 33 s
Test frequency	5 Hz
Displacement amplitude	100 μm
Normal loading	10 N
Lubrication	(1) Saline; (2) Eye drop
Number of wear cycles	20×10^3, 5×10^3, 2×10^4

the test was completed, the surface of the PMMA was scanned. To ensure accurate and reliable results, the test for each parameter was repeated at least three times.

3 Results

3.1 Characterization of Laser-Treated PMMA

3.1.1 White-Light Interferometer

A white-light interferometer was used to compare PMMA at various laser treatment times. The 3D morphological characteristics of the material surface are shown in Figure 3. As shown in Figure 3, the surface was uneven, small bumps and depressions were evident, and the pits became more noticeable as the treatment time increased. Figure 4 shows the wear scars of PMMA treated with an excimer laser. Surface roughness increased with increasing processing time. The depth of the wear scars increased significantly with increasing laser-processing time, particularly at $t = 18$–33 s.

3.1.2 Contact Angle Determination

Measuring the contact angle is important for determining the wetting performance of a material surface and is also an important technical means of detecting the material surface [31]. After the two liquids were sprayed into the PMMA zone, droplets formed (Figure 5). The contact angle can be expressed by Eq. (1).

$$\cos\theta = \frac{\gamma s - \gamma sl}{\gamma l}, \tag{1}$$

where θ is the contact angle, and γs, γl, and γsl refer to the surface tensions of the vapor, liquid, and solid, respectively. Saline solution and 0.1% sodium hyaluronate eye drops (hereinafter, "eye drops") were selected as measurement lubrication conditions, and the volume of liquid per experiment was 2 μL. The wetted pictures in Figures 6 and 7 were processed and analyzed to obtain the contact angle. The wetting contact angle of each sample was the average of three sets of measurements. The experimental results indicate that a change in the liquid did not significantly change the surface physical properties of the material. The materials had hydrophilic surfaces ($\theta < 90°$) with similar wetting contact angles. However, in the eye drop environment, the contact angle was significantly reduced compared with that in saline solution (Figure 8). The results show that the surfaces of the PMMA materials after excimer laser treatment were more hydrophilic. The hydrophilic material was more adsorptive and formed a thick film to reduce friction, which was presumably involved in the composition of the material wear mechanism.

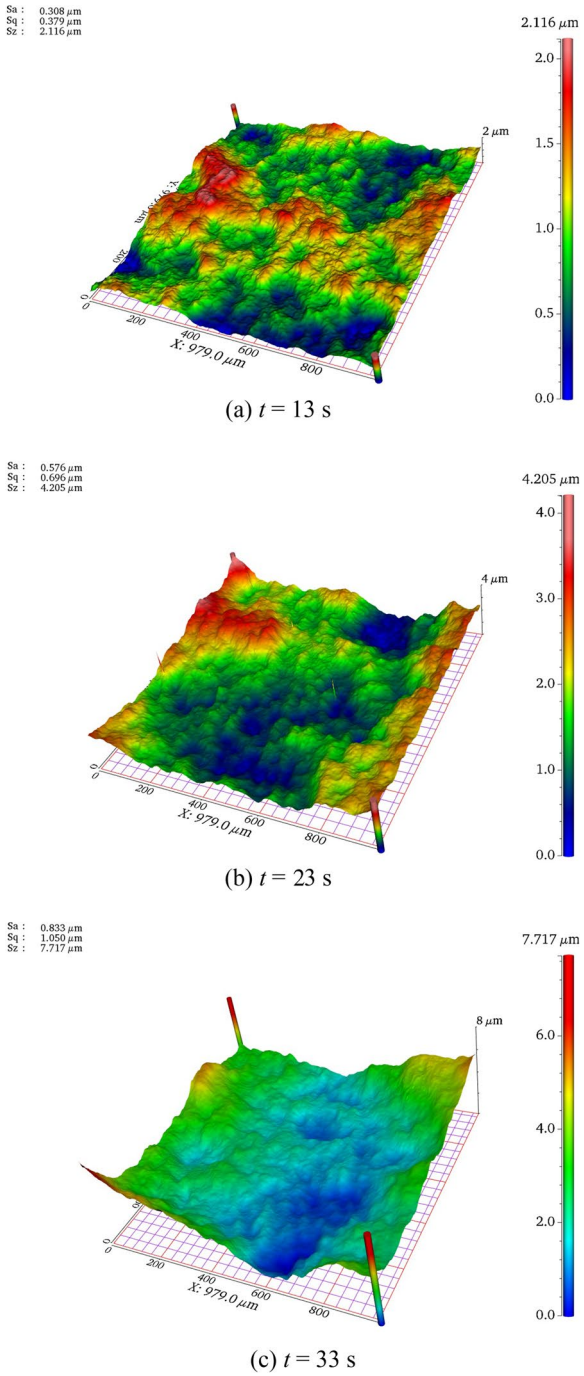

Figure 3 Morphology of the PMMA surface under various laser-processing times

3.1.3 Raman Spectra

The Raman spectrum is a scattering spectrum that characterizes the vibration and rotation information of molecules. It can provide precise microstructure information on molecules and has been widely used in the analysis of substance structures. The number, intensity,

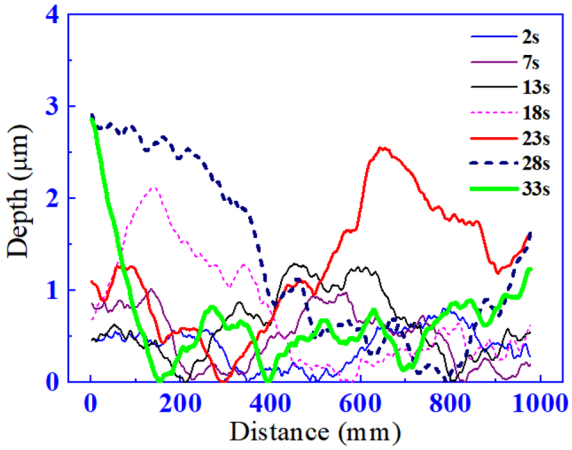

(a) 1/4 line (left position)

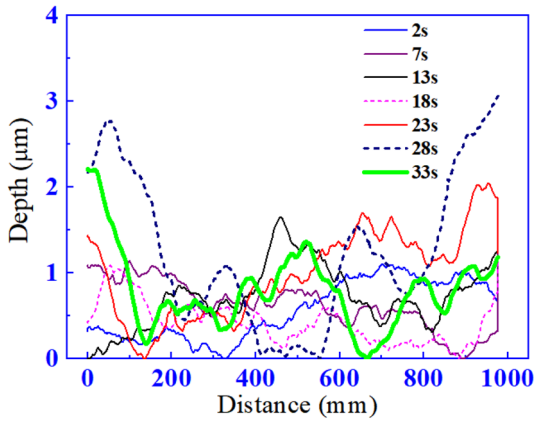

(b) 2/4 line (middle position)

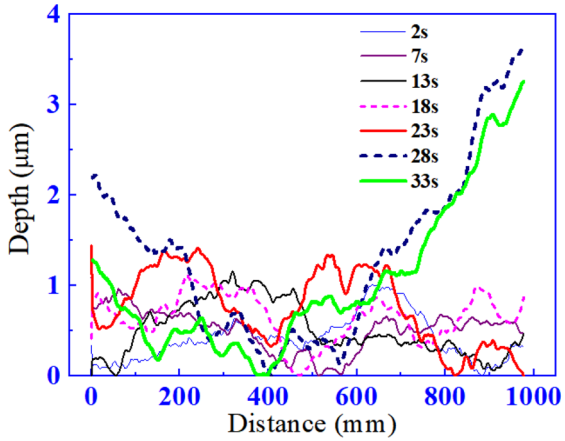

(c) 3/4 line (right position)

Figure 4 Surface section profile of the laser-treated PMMA at different positions

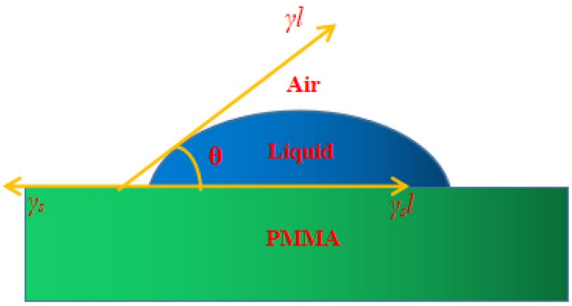

Figure 5 Schematic of contact angle

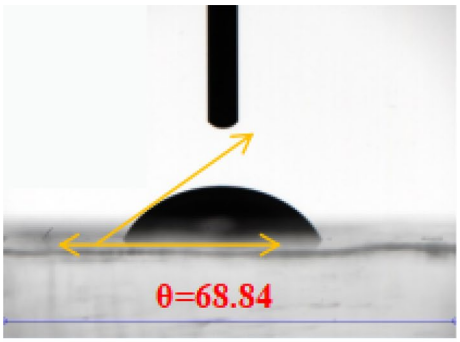

(a) t = 0 s

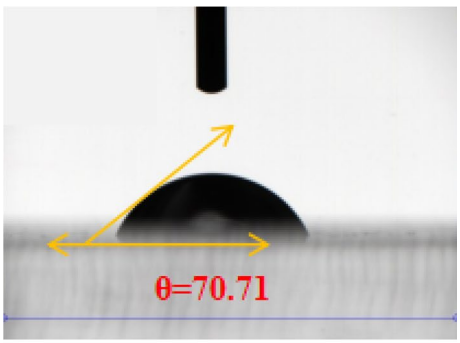

(b) t = 13 s

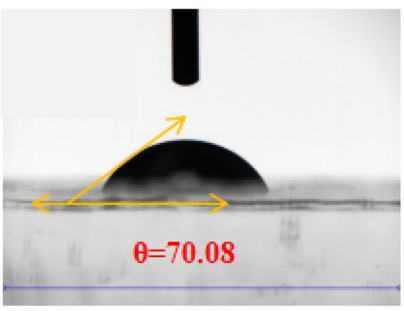

(c) t = 33 s

Figure 6 Contact angle morphology of the PMMA treated at varied laser-processing times in saline solution

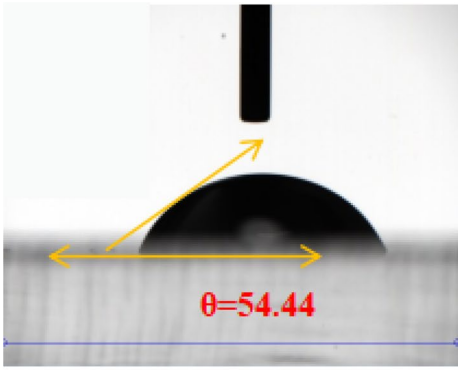

(a) $t = 0$ s

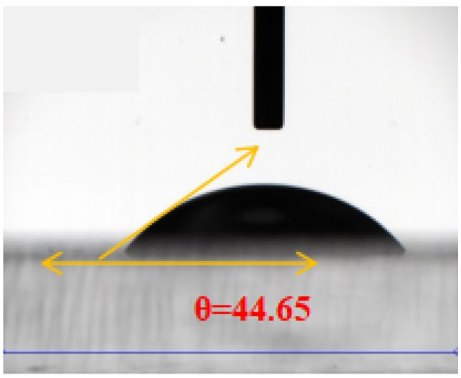

(b) $t = 13$ s

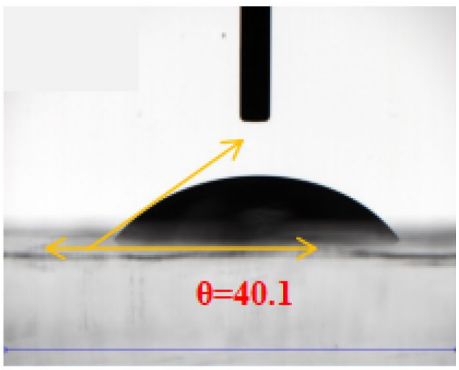

(c) $t = 33$ s

Figure 7 Contact angle morphology of the PMMA treated at varied laser-processing times in eye drop

and frequency displacement of the bands in the spectrum are related to the vibrational and rotational energy levels of the molecules, and the absorption peaks mainly originate from changes in molecular polarizability. After laser treatment, the Raman spectra of the PMMA were observed. The material was identified and quantitatively analyzed by comparing the typical Raman characteristic peaks and their peak strengths. As shown in Figure 9, no significant new peaks appeared as the laser-processing time increased. However, two distinct peaks of the

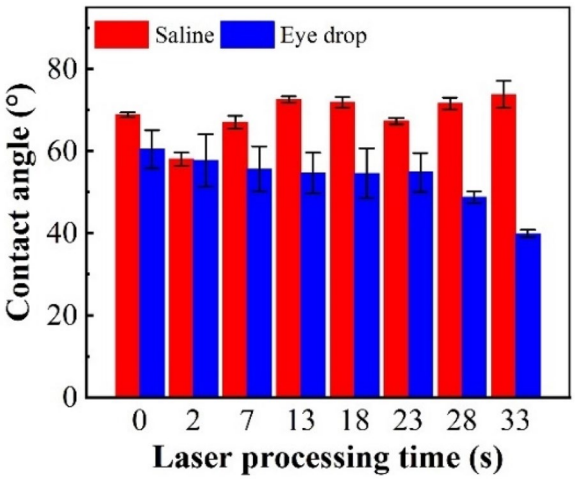

Figure 8 Contact angle changes of the PMMA in different lubrication conditions

Raman spectra of the materials appeared at 800 and 3000 cm^{-1}. Thus, one can infer that the excimer laser increases the roughness of the material and may change the internal arrangement of the molecule, but it does not produce new chemical changes. This finding indicates that the laser breaks the existing chemical bonds in the organic compound molecules and does not form new chemical bonds and groups.

3.2 Influence of Laser Treatment on Wear Behavior

3.2.1 Surface Topography Analysis

Figures 10 and 11 show the 3D topography of PMMA in saline and eye drop environments at various laser-processing times. The round pit structure had a clear edge after wear, and the bottom of the round pit was relatively flat. The patterns after laser processing differed on different initial surfaces. As shown in Figure 10, the bottoms of the micropits were smooth, and the scrubs were pushed out to the periphery. However, the pits did not deepen with wear, indicating that they were filled with abrasive debris. As shown in Figure 10, in the case of liquid lubrication, the round pit texture stored liquid and debris and reduced the actual contact area [32].

As Figure 11 shows, it was difficult to discharge the debris outside the wear area. The surrounding wear area boundary was clear, with debris accumulating in the central zone. Figure 11 reveals that the debris was pushed into different positions during wear processing, indicating that the pits were divided by the debris with force. The pits also became smaller, as shown in Figure 11c, as if they were constantly filled with abrasive debris.

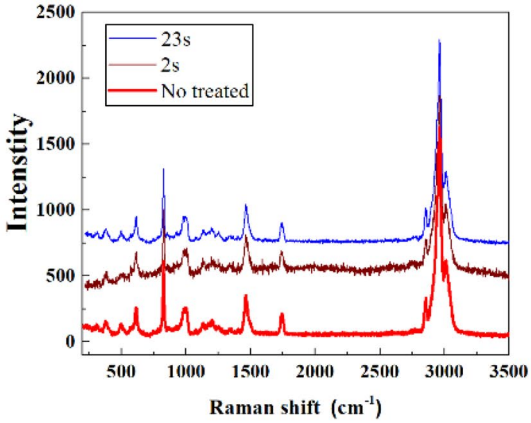

(a) Raman shift

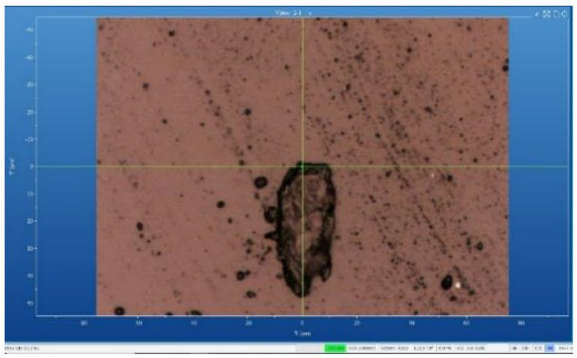

(b) $t = 2$ s

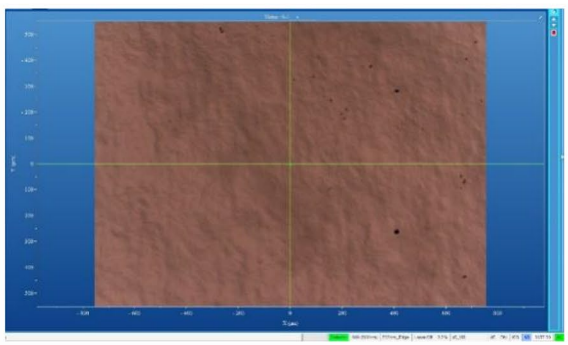

(c) $t = 23$ s

Figure 9 Raman spectra of PMMA surfaces after laser treatment

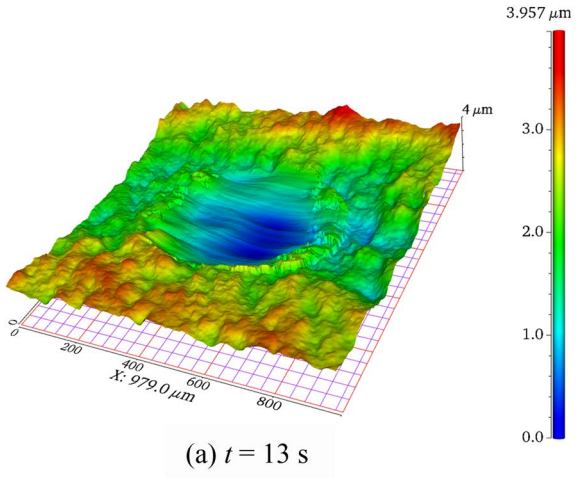

(a) $t = 13$ s

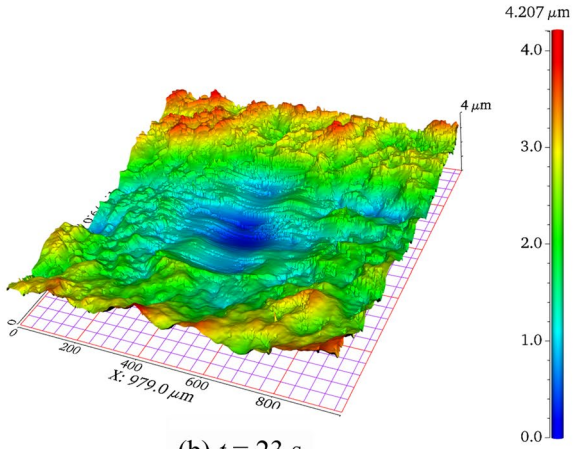

(b) $t = 23$ s

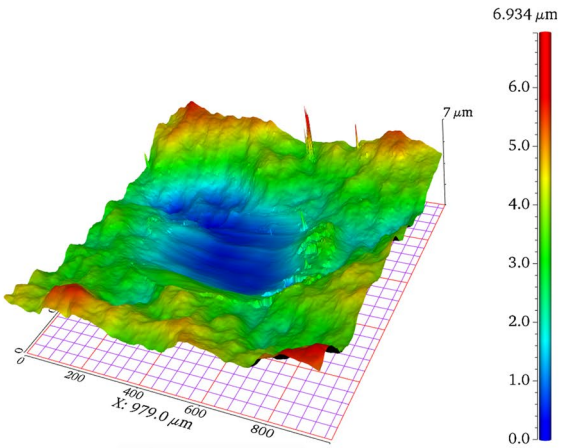

(c) $t = 33$ s

Figure 10 Three-dimensional morphologies of the wear scars of PMMA under various laser treatment times in saline solution

The differences in the 3D morphology further demonstrate that the morphologies of the debris may not be the same at different stages of wear friction. After prolonged friction and wear processes, the formation and accumulation of debris and the film layers on the friction surfaces may play an important role in the mechanism of wear friction.

Figure 12 shows profiles of the wear scars on different laser-treated surfaces in the saline and eye drop environments. As shown in Figure 12a, the sliding of different laser-treated PMMA under saline conditions resulted in moderate microscuffing wear behavior, as

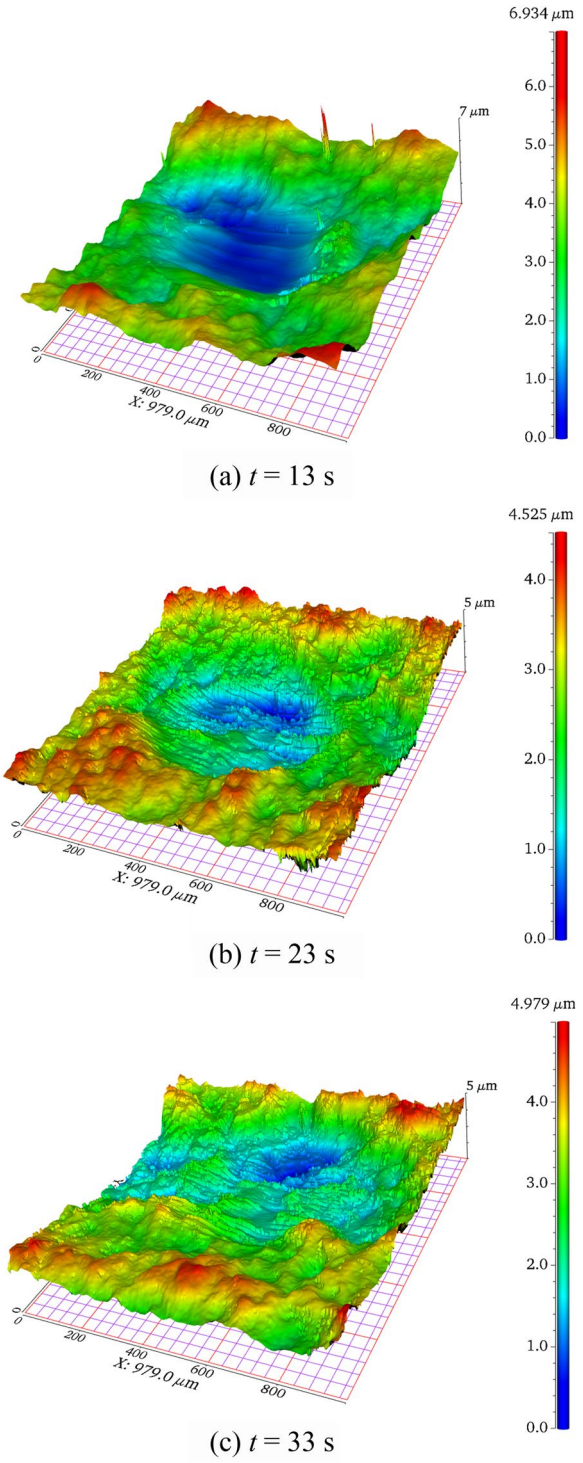

Figure 11 Three-dimensional morphology of laser-treated PMMA after wear friction in eye drop

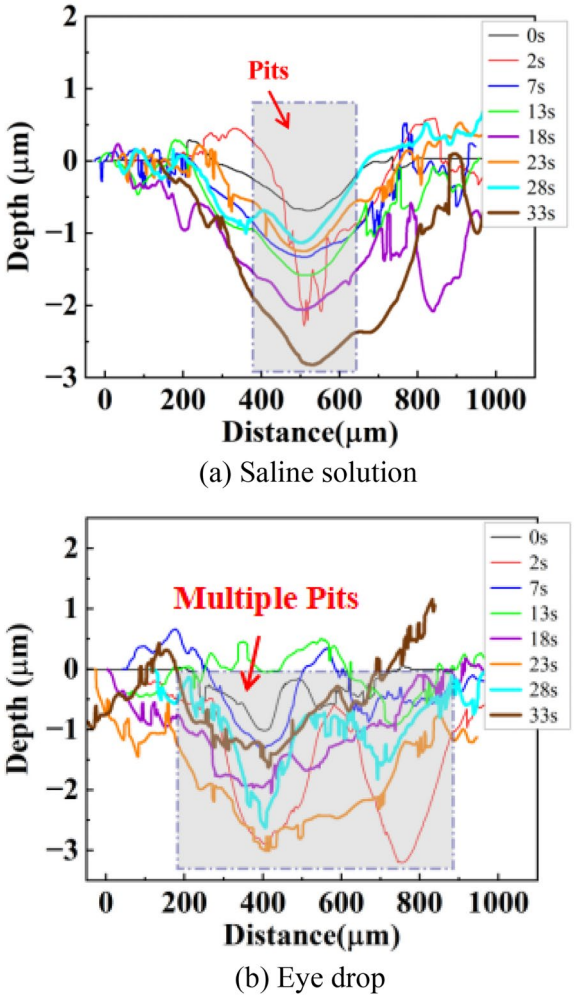

Figure 12 Profiles of the wear scars on laser-treated PMMA under different lubrication conditions

revealed by the roughening and grooves that formed on the wear tracks compared with the smooth surface outside the laser treatment. As shown in Figure 12b, debris particles accumulated considerably on the wear surface, as indicated by the formation of hills with different step heights and widths. However, the extent of this accumulation was significantly lower for the PMMA in saline solution. In addition, the wear in the saline environment created larger wear grooves and pits with a depth of 3 μm on the surface. In contrast, fewer smaller grooves formed on the surface under the eye drop condition.

This behavior can be explained by the relationship between the film layer and debris accumulation. From the aforementioned morphology of the abrasion scars, one can conclude that such a morphology is like a "V" shape under the saline lubrication condition, except for the special case of a crater when the laser treatment time is 2 s, as shown in Figure 12a. The surface is more thoroughly discharged at this time. When the lubrication condition was eye drops, the abrasion contour was more irregular and uneven. However, in the central area,

multiple approximately "W"-shaped pits appeared, as shown in Figure 12b, indicating that the abrasive chips were pushed out but not as easily discharged as in saline solution at this time.

3.2.2 Friction Coefficient

Figure 13 shows the evolution of the friction coefficient versus sliding time for different laser-treated PMMA samples under saline and eye drop conditions. With the extension of the laser treatment time, the friction coefficient exhibited a running-in behavior followed by a steady-state condition, which was caused by the softening of the friction area under the frictional heat generated by high-frequency micromotion, resulting in adhesion on the surface of the material [33]. Figure 13a indicates that the friction coefficient fluctuated noticeably and increased linearly in the early stage because of the uneven material surface caused by the laser treatment, thus generating a high contact stress and shear force on the materials. Subsequently, the materials were in contact with each other and became rapidly worn in a short time. The materials formed a film layer, and the debris that filled the pits worked on the friction surfaces during the stable wear stage with a constant friction coefficient of 0.2, demonstrating the water lubrication characteristics of the laser-treated PMMA. Figure 13b shows that the coefficient of friction of PMMA was significantly reduced in the eye drop environment compared with that in the saline environment, indicating that the accumulated debris formed a layer under a relatively chemically complex lubrication system, leading to a reduction in friction. The smaller frictional force may also result from the formation of finer abrasive debris in the eye drop environment [34, 35].

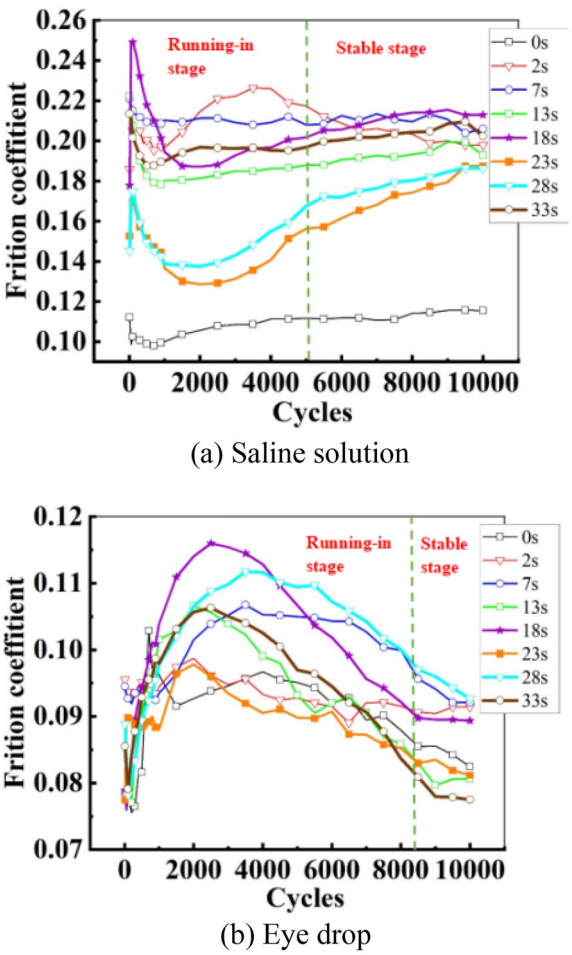

Figure 13 Friction coefficients of laser-treated PMMA under different lubrication conditions

3.2.3 Wear Behavior

The wear rate is calculated [36] as

$$K = \Delta V / FN \cdot L, \tag{2}$$

where K is the specific wear rate of the composite material; ΔV is the wear volume; FN is the load; L is the total stroke. Figure 14a shows the variation in the wear rate of the laser-treated PMMA after experiments under different conditions. Unlike the coefficient of friction, which is larger than that of saline in a solution environment with a relatively complex chemical composition, such as eye drops. This is the opposite trend to the change in wear rate, indicating that the laser-treated material shows a change in wear reduction without wear under eye drop lubrication. As the wear parameters shown in Figures 14b and c reveal that the initial wear of the material was essentially identical under both lubrication conditions, and there was no obvious pattern in the change of wear parameters in the saline environment with the extension of the laser treatment time. Under the eye drop lubrication condition, the wear amount and wear area gradually increased until a laser treatment time of 28 s. However, a decrease occurred at 33 s. In addition, the initial wear rate was essentially identical under both lubrication conditions, and the total wear amount was essentially identical. Combined with the experimental results, it is speculated, based on Archard's law [37], that the unevenness of the friction surface may gradually decrease throughout the wear phase. The wear resistance of the laser-treated PMMA in physiological saline improved significantly.

3.2.4 Scanning Electron Microscopy Analysis

Scanning electron microscopy (SEM) was used to observe the wear scars produced by the excimer laser [38]. The SEM images of the microstructures of the worn surfaces of PMMA processed using the excimer laser are

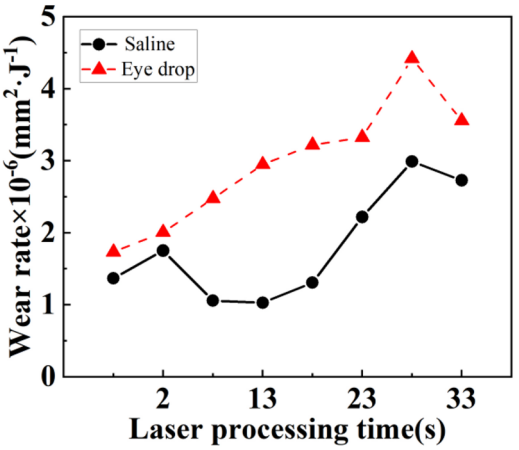

(a) Wear rate

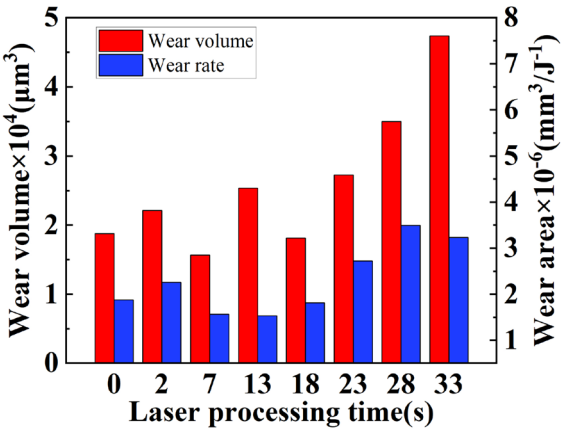

(b) Saline solution

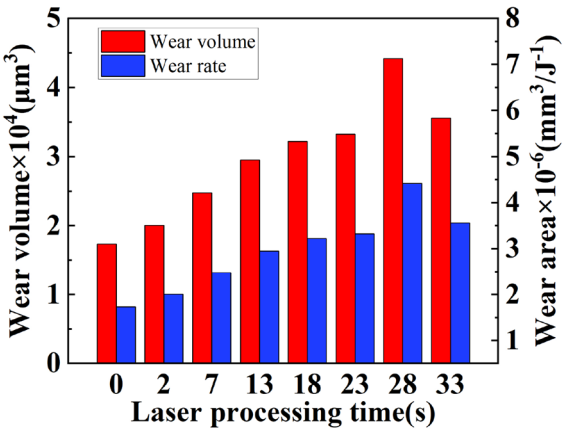

(c) Eye drop

Figure 14 Wear statistics of laser-treated PMMA under different lubrication conditions.

shown in Figure 15. The wear track of the PMMA surface exhibited white cracks and grooves parallel to the circle, as shown in Figure 15a. The spalling and white cracks shown in Figures 15b and c occurred at the material base and radiated to the debris accumulation layer, probably because of wear stress transformation and delamination. The plow in Figures 15d and e created by the plowing action of wear debris suggest the occurrence of abrasive wear of the materials, and the patch came from the adherence of the debris, as shown in Figure 15e. The wear morphology of the PMMA differed with the laser-processing time by showing more plows and adhesions, as shown in Figures 15e and f, and significant spalling was caused by the wear behavior shown in Figure 15h. Pits formed intensively on the surface, as shown in Figure 15g, either acting as third-body abrasive particles or washing away from the interface. Pits also formed loosely because the moving debris collided with the embedded debris, stopping the formation of a continuous groove on the coating.

3.3 Influence of Cycle Times on Wear Behavior

The friction–displacement (*Ft–D*) curve and friction coefficient are the main parameters in microprocessing. The *Ft–D* curve reflects the macrodynamic motion state of the material. Figure 16 shows the *Ft–D* curves for different cycle numbers. When the shape of the macrocycle diagram is a straight line or an ellipse, the microwear is in the partial slip zone. When the macrocycle diagram is a parallelogram, the microwear is in the slip zone [39]. When the displacement amplitude is unchanged (D = 100 μm), the *Ft–D* curves under the three cycle numbers (2000, 5000, and 20,000) are basically parallelograms, indicating the relative slip of the contact surface, which is defined as the complete slip mechanism, known as the "gross slip regime" (GSR) [40]. The abrasive debris in fretting wear may act as abrasive particles, which aggravate wear or adhere to the contact surface to form a film that can shear and deform on the contact surface, thereby buffering the sliding between the contact surfaces [6]. If the abrasive wear is dominant, the presence of abrasive debris promotes wear. If adhesive wear is dominant, the anti-adhesion effect provided by the wear chip is greater than the effect of the abrasive wear it causes, and the presence of the wear chip inhibits wear [22]. The friction wear mechanism of the laser-treated PMMA samples in different solutions was further examined by changing the number of friction cycles.

3.3.1 Friction Coefficient

After the number of cycles was changed, the friction coefficients still showed typical running-in and stable stages, despite some differences in Figures 17a and b. In

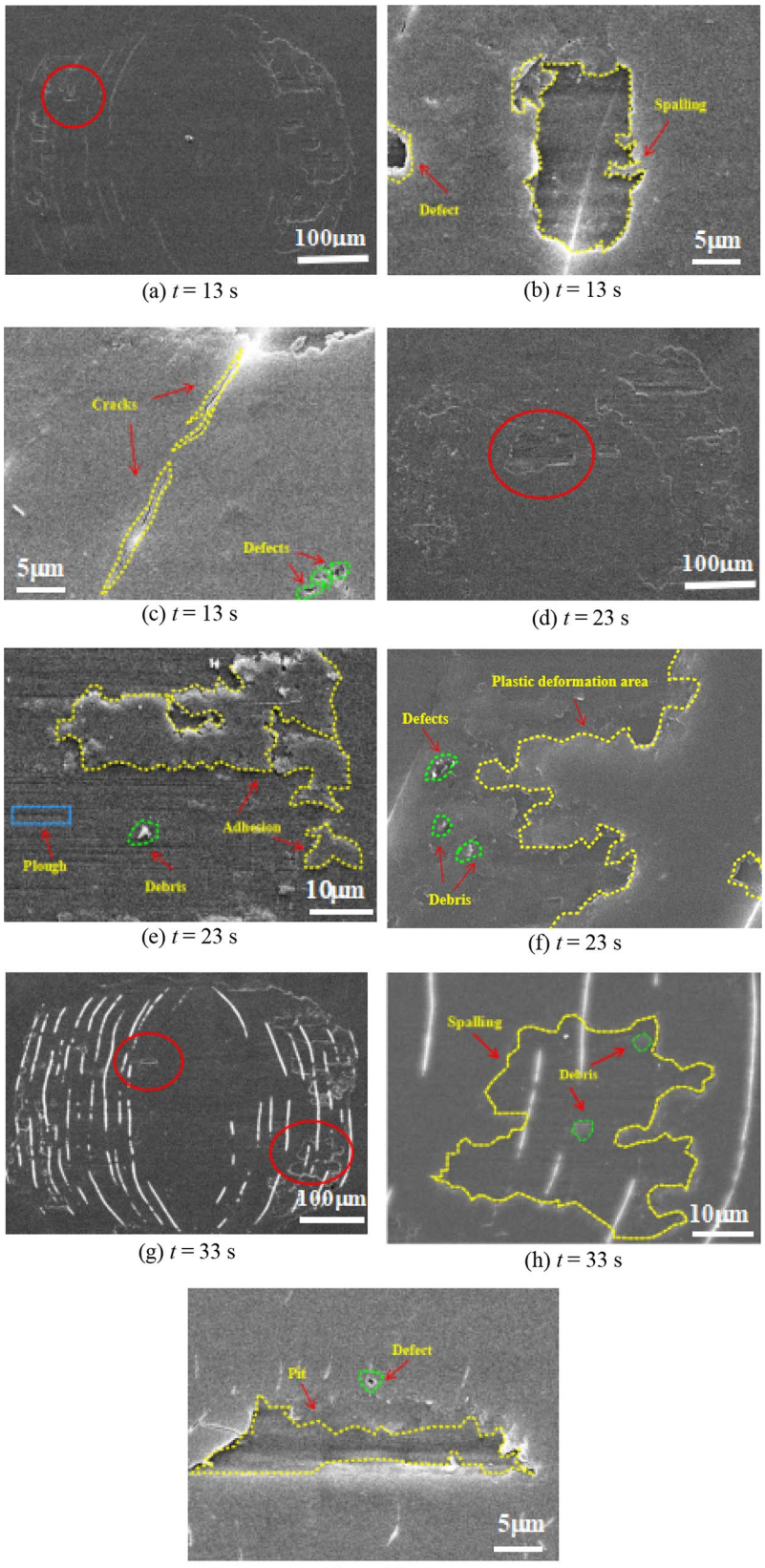

Figure 15 SEM morphologies of worn surfaces in PMMA with various laser treatments

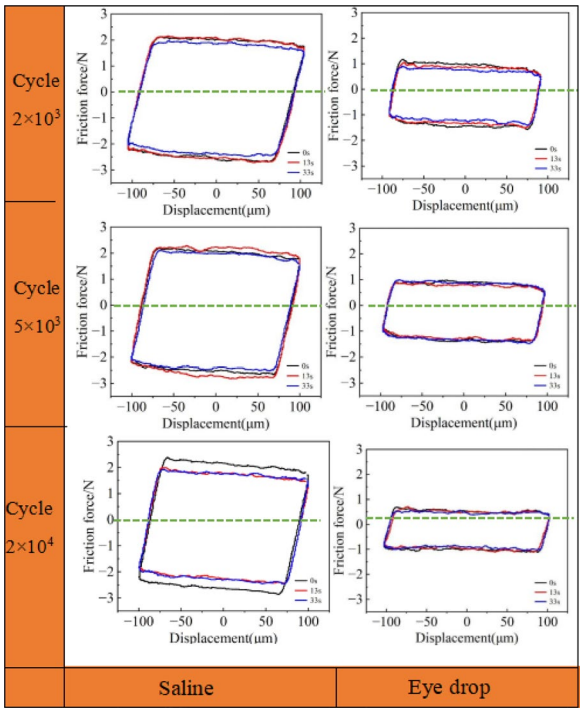

Figure 16 *Ft–D* curves of laser-treated PMMA under different lubrication conditions and different cycle numbers

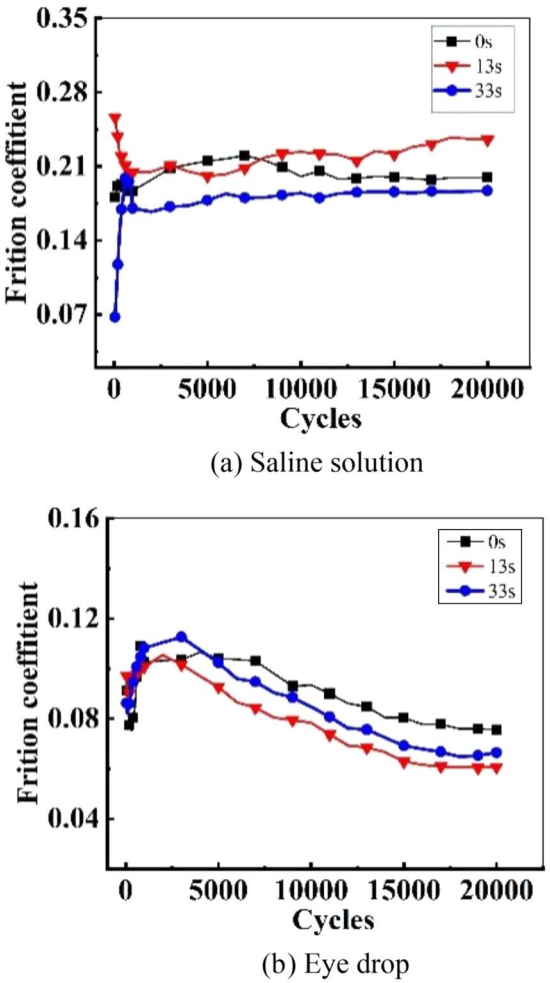

Figure 17 Friction coefficients in various lubrication conditions of laser-treated PMMA

different environments, the friction coefficients of the samples reached a steady state after the running-in stage. The running periods experienced when entering the steady state differed. Moreover, in the same liquid environment, the friction coefficient did not fluctuate significantly. The contact surface gradually changed from a two-body to a three-body action. The friction coefficient first increased, then decreased, and remained relatively stable when the generation of the third body (abrasive chip layer) and the overflow from the surface maintained dynamic equilibrium.

3.3.2 Effect of Cycles on Wear Behavior

As shown in Figures 18 and 19, the morphology and profile of the material changed significantly with increasing cycle time. The wear scars of the laser-treated material were smoother in the saline environment (Figure 18). Large pits appeared at 20,000 cycles when material accumulation was evident around the periphery. The maximum depth of the abrasion scar occurred at 5000 cycles in the saline environment, close to 4 μm. In the eye drop environment (Figure 19), the material surface was rougher and the abrasion depth and width were smaller than those in saline, but the number of scars increased. Significant accumulation of the material occurred after 5000 cycles, and the maximum abrasion depth occurred after 20000 cycles.

The materials exhibited different wear characteristics as the number of friction cycles increased. Figure 20 shows a comparative quantitative analysis of the wear volume and wear rate as the number of cycles changed. With an increase in the cycle time, the wear volume changed significantly, as shown in Figure 20. Under both lubrication conditions, the wear rate increased with increasing laser treatment time. For saline lubrication, the wear rate decreased with increasing cycle time. For eye drop lubrication, the wear rate first increased and then decreased with increasing laser treatment time.

4 Wear Mechanism

When PMMA was treated with an excimer laser under different lubrication conditions, the surfaces and profiles changed significantly, as shown in Figures 5, 6, 7, 8. The

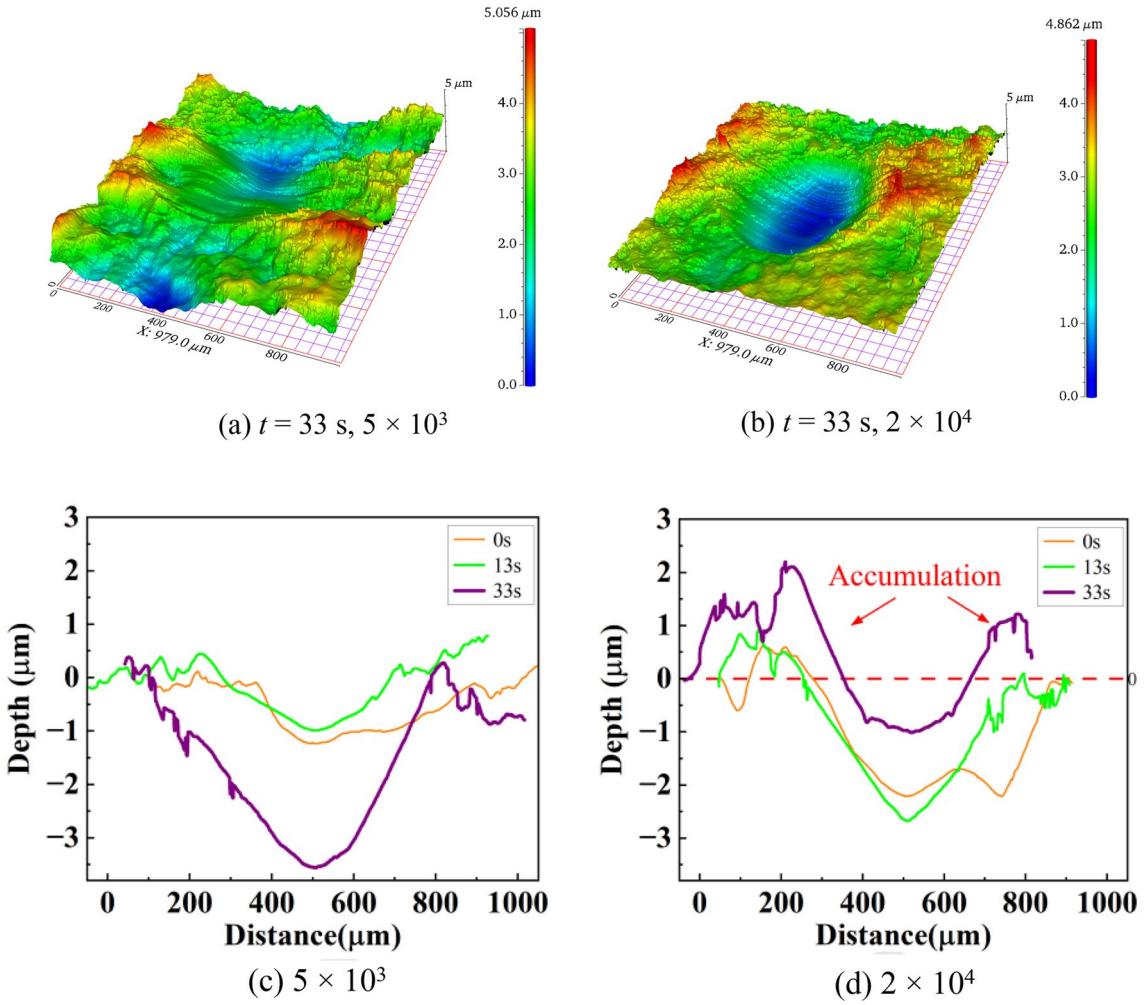

Figure 18 Three-dimensional morphologies and profiles of wear scars of the laser-treated PMMA in saline solution with different cycle numbers

materials became more hydrophilic. As shown in Figure 16, the material exhibited typical GSR morphological characteristics. As shown in Figures 10 and 11, the surfaces treated by the excimer laser were covered by a layer that exhibited plastic deformation, also known as the "third layer." However, the debris in saline and eye drop conditions showed significant differences in wear behavior. Debris detached from the contact surface, and multiple plowing grooves along the fretting direction were observed using SEM, as shown in Figure 15.

Yamakirin et al. [12] investigated the effects of laser surface texturing on the friction behavior of silicon nitride under water lubrication. They found that, in the case of a small textured surface, pits were buried with the wear debris. Similarly, for PMMA materials treated by an excimer laser under different lubrication conditions in the wet process, the contact area increases with time, and several pieces of debris are generated or patched by wear behavior. Meanwhile, debris rolling with the liquid fills the pits and grooves on the surface, either in the center or at the periphery. Therefore, the surface may be flattened by a combination of factors, resulting in a decreased friction coefficient (Figure 14). Different liquid environments change the mode of the debris, resulting in different changes in the friction coefficient and wear rate. The abnormal phenomenon of a high wear rate in the eye drop environment may result from the complex chemical composition, which may reduce the stress concentration. Changing the friction cycle causes the debris and flakes to destroy the membrane of the worn surface produced during the wear process, thus weakening the lubrication effects of the third layer. The contact area increases, improving the friction coefficient (Figure 17). The steady lubrication layer protects the materials from laser modification and can reduce the friction area and lubricate the wear.

Figure 14d shows flaking pits caused by contact fatigue and trenches caused by abrasive wear, indicating the

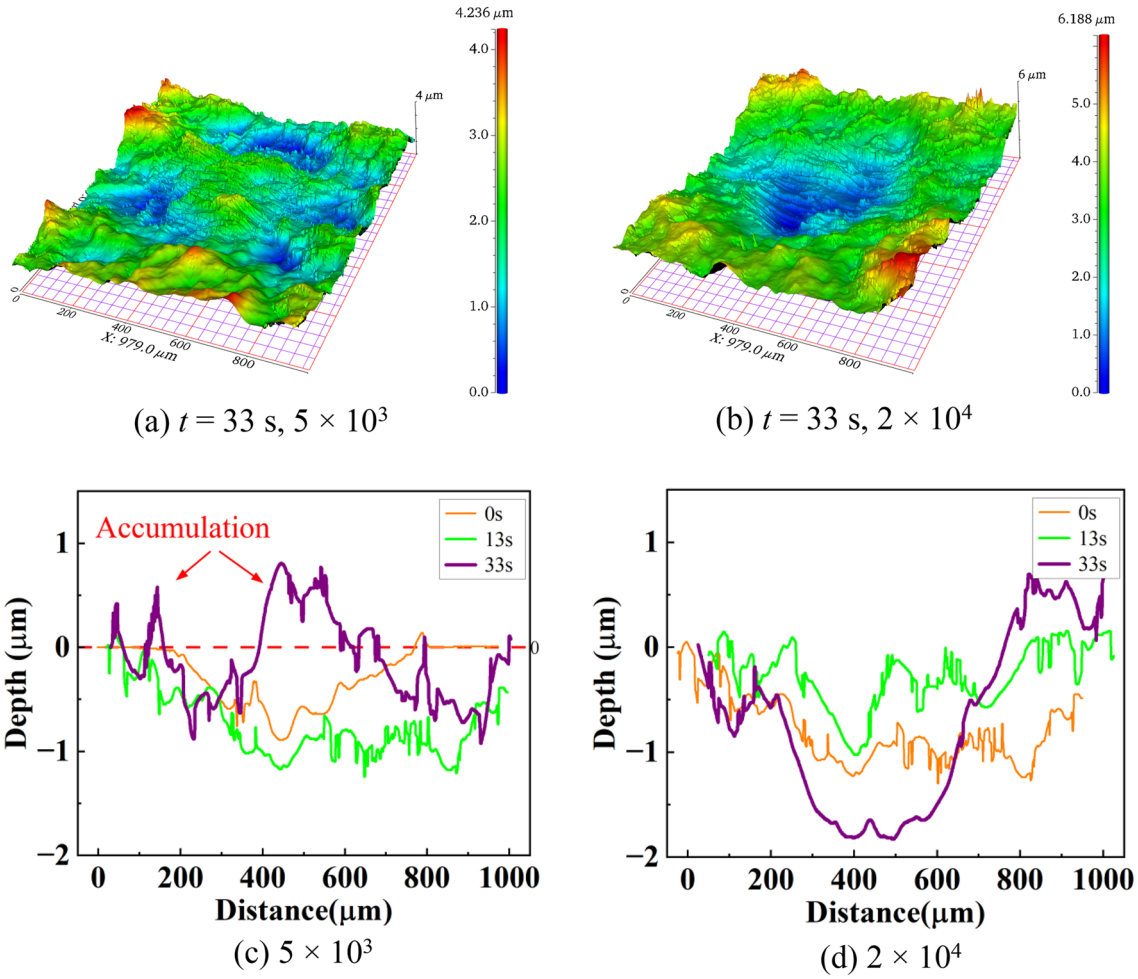

Figure 19 Three-dimensional morphologies and profiles of wear scars of laser-treated PMMA in eye drop with different cycle numbers

occurrence of surface fatigue and abrasive wear. The 3D morphology of the wear scars shows a significant material deformation in the contact area, with a maximum wear depth of nearly 4 μm. The profile of the scars (Figures 12 and 18) partially shows a "V" or "W" shape, indicating a relatively typical change in the form of exclusion and accumulation of abrasive debris.

This analysis indicates that several wear mechanisms can occur simultaneously during the wear process (Figure 21).

5 Conclusions

(1) The laser surface texture has the following effects on the friction behavior of excimer-laser-treated PMMA: the roughness of the material increases, the physical structure changes, and the material becomes more hydrophilic. In lubricated environments with more-complex chemical compositions, such as eye drops, the friction coefficient of the material decreases, but the wear rate increases. It is speculated that this is caused by the involvement of eye drops in the formation of finer abrasive chips during the wear of the laser-treated material or by the formation of a new film because of the abrasive debris. In conclusion, the material is more resistant in a saline environment.

(2) During fretting wear, both the number of cycles and the laser treatment affect the wear mechanism. In a state of complete slip, wear mainly takes three forms. 1) The wear debris generated is not quickly discharged from the contact zone but forms a third body layer, which covers the contact surface with the transfer film, at which time the wear is small.

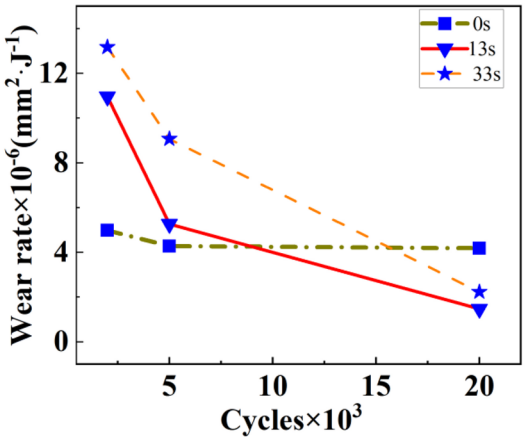

(a) Saline solution

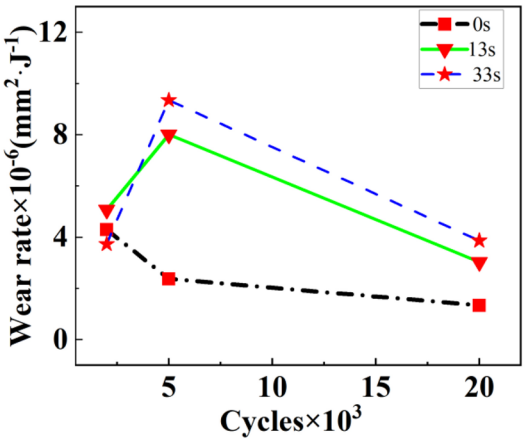

(b) Eye drop

Figure 20 Wear statistics of laser-treated samples under different friction cycle numbers

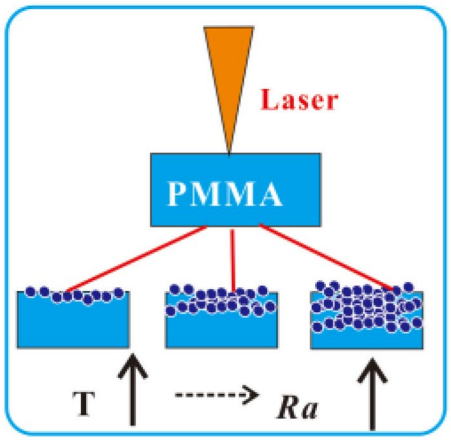

(a) Laser treatment processing

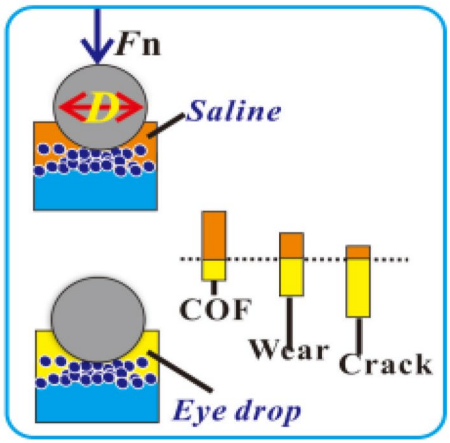

(b) Wear mechanism

Figure 21 Schematic representations of wear of laser-treated PMMA in different lubrication conditions

2) Surface fatigue wear occurs. As the friction progresses, the grinding debris acts as a third body. The appearance of wear marks reduces the actual contact area and friction coefficient, reducing the tangential friction. The denaturation of the material further reduces the friction of the transfer film cover. 3) Abrasive wear occurs. The accumulation of abrasive debris and the destruction of the transfer film (or the involvement of lubrication condition components) increase the exposure and denaturation of the material and increase wear.

Acknowledgements
Not applicable.

Author Contributions
DQ and WH were in charge of the entire trial. DQ wrote the manuscript; DQ, JG, LC and ML assisted with sampling and laboratory analyses. All authors read and approved the final manuscript.

Authors' information
Dong Qin born in 1984, is currently a PhD candidate at *West China Hospital, Sichuan University, China*, and received his Master's degree in ophthalmology from *Southwest Medical University, China*, in 2011.
Juan Guo born in 1971, is currently the chief ophthalmology department at *The Third People's Hospital of Chengdu, China*. She graduated from *Southwest Medical University, China*, in 1994. His research interests include intraocular implants and biomaterials.
Ming Liang born in 1975, is currently a professor of ophthalmology at *The Third People's Hospital of Chengdu, China*. He received his Master's degree from

West China Hospital, Sichuan University, China, in 2007. His research interests include ophthalmic biomaterials, intraocular implants, and the prevention and control of myopia among adolescents.
Ling Chen born in 1988, is currently a senior ophthalmic technician at *The Third People's Hospital of Chengdu*, China. He graduated from *North Sichuan Medical College, China*, in 2011.
Weimin He born in 1969, is currently a professor and leading researcher at *West China Hospital, Sichuan University, China*. She graduated from *the Department of Medicine, West China University of Medical Science, China*, with a six-year bachelor's degree. She received her master's degree in ophthalmology from *West China University of Medical Sciences, China*, in 1999 and her doctoral degree in ophthalmology from *Sichuan University, China*, in 2004. She has published 103 papers by the first author and corresponding author and edited (translated) 16 textbooks and monographs. Her research interests include ocular tumors, ophthalmic biomaterials, and intraocular materials.

Funding
Supported by the Chengdu Municipal Medical Research Project (Grant Nos. 2019005 and 2022014) and Sichuan Provincial Cadres Health Research Project (Grant No. ChuanGanYan (2013-104)).

Availability of Data and Materials
The datasets supporting the conclusions of this article are included within the article.

Declarations

Competing Interests
The authors declare no competing financial interests.

Received: 16 February 2023 Revised: 18 August 2023 Accepted: 24 August 2023
Published online: 19 September 2023

References

[1] S Resnikoff, V C Lansingh, L. Washburn, et al. Estimated number of ophthalmologists worldwide (International Council of Ophthalmology update): will we meet the needs? *British Journal of Ophthalmology,* 2020, 104(4): 588-592.
[2] Shuaijun Zhang, Junqiu Zhang, Bin Zhu, et al. Progress in bio-inspired anti-solid particle erosion materials: Learning from nature but going beyond nature *Chin. J. Mech. Eng.,* 2020, 33: 42.
[3] C De las Heras Alarcón, S Pennadam, C J C S R Alexander. Stimuli responsive polymers for biomedical applications. *Chemical Society Reviews,* 2005, 34(3): 276-285.
[4] N K Guimard, N Gomez, C E Schmidt. Conducting polymers in biomedical engineering. *Progress in Polymer Science,* 2007, 32(8-9): 876-921.
[5] B D Ulery, L S Nair, C T Laurencin. Biomedical applications of biodegradable polymers. *J Polym Sci B Polym Phys,* 2011, 49(12): 832-864.
[6] A Ralls, P Kumar, M Misra, et al. Material design and surface engineering for bio-implants. *Jom,* 2020, 72(2): 684-696.
[7] J W Cheng, R L Wei, J P Cai, et al. Efficacy of different intraocular lens materials and optic edge designs in preventing posterior capsular opacification: a meta-analysis. *Am J Ophthalmol,* 2007, 143(3): 428-436.
[8] U Ali, K J B A Karim, N A Buang. A review of the properties and applications of poly (methyl methacrylate)(PMMA). *Polymer Reviews,* 2015, 55(4): 678-705.
[9] C XIA, X FAN, C DING, et al. Experimental about pyrolysis of poly (methyl methacrylate) in a fluidized-bed reactor. *Chinese Journal of Environmental Engineering,* 2016, 10(11): 6669-6672.
[10] D T Beruto, R Botter, M Fini. The effect of water in inorganic microsponges of calcium phosphates on the porosity and permeability of composites made with polymethylmethacrylate. *Biomaterials,* 2002, 23(12): 2509-2517.
[11] A Isha, N A Yusof, M Ahmad, et al. A chemical sensor for trace V (V) ion determination based on fatty hydroxamic acid immobilized in polymethylmethacrylate. *Sensors Actuators B: Chemical,* 2006, 114(1): 344-349.
[12] S Mishra and G Sen. Microwave initiated synthesis of polymethylmethacrylate grafted guar (GG-g-PMMA), characterizations and applications. *International Journal of Biological Macromolecules,*2011, 48(4): 688-694.
[13] H Yamakiri, S Sasaki, T Kurita, et al. Effects of laser surface texturing on friction behavior of silicon nitride under lubrication with water. *Tribology International,* 2011, 44(5): 579-584.
[14] J Kost, R Langer. Responsive polymeric delivery systems. *Advanced Drug Delivery Reviews,* 2012, 64: 327-341.
[15] B Osi, M Khoder, A A Al-Kinani, et al. Pharmaceutical, biomedical and ophthalmic applications of biodegradable polymers (BDPs): literature and patent review. *Pharm Dev Technol,* 2022, 27(3): 341-356.
[16] E van der Worp, D Bornman, D L Ferreira, et al. Modern scleral contact lenses: A review. *Cont Lens Anterior Eye,* 2014, 37(4): 240-250.
[17] S Patel, R G Thakar, J Wong, et al. Control of cell adhesion on poly (methyl methacrylate). *Biomaterials,* 2006, 27(14): 2890-2897.
[18] D S Bodas, C Khan-Malek. Fabrication of long-term hydrophilic surfaces of poly (dimethyl siloxane) using 2-hydroxy ethyl methacrylate. *Sensors Actuators B: Chemical,* 2007, 120(2): 719-723.
[19] M J Colthurst, R L Williams, P S Hiscott, et al. Biomaterials used in the posterior segment of the eye. *Biomaterials,* 2000, 21(7): 649-650.
[20] P K Chu, J Chen, L Wang, et al. Plasma-surface modification of biomaterials. *Materials Science Engineering: R: Reports,* 2002, 36(5-6): 143-206.
[21] T Ito, S Kuno, T Uchida, et al. Properties and reactivity of the adenosine radical generated by radiation-induced oxidation in aqueous solution. *J Phys Chem B,* 2009, 113(1): 389-394.
[22] K Iwamatsu, S Sundin, J A LaVerne. Hydrogen peroxide kinetics in water radiolysis. *Radiation Physics and Chemistry,* 2018, 145: 207-212.
[23] A Tegze, G Sagi, K Kovacs, et al. Radiation induced degradation of ciprofloxacin and norfloxacin: Kinetics and product analysis. *Radiation Physics and Chemistry,* 2019, 158: 68-75.
[24] J T Busby, G S Was, E A Kenik. Isolating the effect of radiation-induced segregation in irradiation-assisted stress corrosion cracking of austenitic stainless steels. *Journal of Nuclear Materials,* 2002, 302(1): 20-40.
[25] M J H Dowlath, S K Karuppannan, P Sinha, et al. Effects of radiation and role of plants in radioprotection: A critical review. *Sci Total Environ,* 2021, 779: 146431.
[26] Z Hua, X Han, G Li, et al. Prevalence and associated factors for climatic droplet keratopathy in Kazakhs adults: a cross-sectional study in Tacheng, Xinjiang, China. *BMC Ophthalmol,* 2021, 21(1): 316.
[27] A Y Vorobyev, C L Guo. Direct femtosecond laser surface nano/microstructuring and its applications. *Laser & Photonics Reviews,* 2013, 7(3): 385-407.
[28] M Hashida, H Mishima, S Tokita, et al. Non-thermal ablation of expanded polytetrafluoroethylene with an intense femtosecond-pulse laser. *Opt Express,* 2009, 17(15): 13116-13121.
[29] D Teixidor, F Orozco, T Thepsonthi, et al. Effect of process parameters in nanosecond pulsed laser micromachining of PMMA-based microchannels at near-infrared and ultraviolet wavelengths. *The International Journal of Advanced Manufacturing Technology,* 2013, 67(5): 1651-1664.
[30] L Pingxue, X Chenggao, G Jian. Research progress and development of picosecond laser processing. *Laser Infrared,* 2018, 48(10): 1195-1203.
[31] X Bai, J Jiang, C Li, et al. Tribological performance of different concentrations of Al_2O_3 nanofluids on minimum quantity lubrication milling. *Chinese Journal of Mechanical Engineering,* 2023, 36: 11.
[32] N Agrawal, S C Sharma. Performance of textured spherical thrust hybrid bearing operating with shear thinning and piezoviscous lubricants. *J Engineering Tribology,* 2022, 236(4): 607-633.
[33] X P Qin, J Li, H Meng, et al. Effects of friction heat on tribological properties of UHMWPE. *Tribology,* 2005, 25(6): 550-554.
[34] J Halliday, W Hirst. The fretting corrosion of mild steel. *Mathematical Physical Sciences,* 1956, 236(1206): 411-425.
[35] S Fayeulle, P Blanchard, L Vincent. Fretting behavior of titanium-alloys. *Tribology Transactions,* 1993, 36(2): 267-275.
[36] M S Wright, V K Jain, C S Saba. Wear rate calculation in the four-ball wear test. *Wear,* 1989, 134(2): 321-334.
[37] J P Chen, Y W Zhu, J B Wang, et al. Relationship between mechanical properties and processing performance of agglomerated diamond abrasive compared with single diamond abrasive. *Diamond and Related Materials,* 2019, 100: 107595.

[38] J G Zhang. Study on friction and wear behavior of PMMA composites reinforced by HCl-immersed TiO2 particles. *Journal of Thermoplastic Composite Materials,* 2014, 27(5): 603-610.
[39] J Wang, D Duan, W Xue, et al. Ti-6Al-4V fretting wear and a quantitative indicator for fretting regime evaluation. *J Engineering Tribology,* 2021, 235(2): 423-433.
[40] X Yuan. Tangential fretting wear behavior of CuMg0.4 alloy. *The Chinese Journal of Nonferrous Metals,* 2022, 32(4): 962-974.